Sulfoxythiocarbamate S-4 inhibits HSP90 in human cutaneous squamous cell carcinoma cells

Zhang, Ying; VanHecke, Garrett C.; Ahn, Young-Hoon; Proby, Charlotte M.; Dinkova-Kostova, Albena T.

Published in:
European Journal of Pharmacology

DOI:
10.1016/j.ejphar.2020.173609

Publication date:
2020

Sulfoxythiocarbamate S-4 inhibits HSP90 in human cutaneous squamous cell carcinoma cells

Ying Zhang[1], Garrett C. VanHecke[2], Young-Hoon Ahn[2], Charlotte M. Proby[1], and Albena T. Dinkova-Kostova[1,3,*]

[1]*Jacqui Wood Cancer Centre, School of Medicine, University of Dundee, Scotland, UK*

[2]*Department of Chemistry, Wayne State University, Detroit, MI, USA*

[3]*Department Pharmacology and Molecular Sciences and Department of Medicine, Johns Hopkins University School of Medicine, Baltimore, MD, USA*

*Address correspondence to: Albena T. Dinkova-Kostova, Division of Cellular Medicine, School of Medicine, Jacqui Wood Cancer Centre, James Arnott Drive, Dundee DD1 9SY, Scotland, United Kingdom. Tel: 44-1382-383386;

Email: a.dinkovakostova@dundee.ac.uk

Abstract

Cancer cells rely heavily on molecular chaperones, such as heat shock protein 90 (HSP90), and their co-chaperones. The development of HSP90 inhibitors is an attractive therapeutic approach that has the potential to affect multiple hallmarks of cancer. Such approach is particularly needed for tumors that carry large mutational burdens, including cutaneous squamous cell carcinomas (cSCC). We previously identified sulfoxythiocarbamate S-4 as an HSP90 inhibitor. In this study, we investigated the mechanism(s) by which S-4 compromises the viability of human cSCC cells. S-4 inhibits HSP90 and causes depletion of its clients HER2, a tyrosine kinase oncoprotein, and Bcl-2, an anti-apoptotic protein. The decrease in Bcl-2 is accompanied by cytochrome c release from mitochondria into the cytoplasm, suggesting apoptosis. In the surviving cells, depletion of the HSP90 clients cyclin D and CDK4 by S-4 prevents phosphorylation of the retinoblastoma protein Rb and the release of transcription factor E2F, inhibiting G1-S cell cycle progression and cell division. These findings illustrate the comprehensive effectiveness of S-4 and encourage future development of compounds of this type for cancer prevention and treatment.

Keywords

cell cycle arrest, electrophile, HSP90, skin cancer

1. Introduction

Heat shock protein 90 (HSP90) facilitates the correct folding and stability of a broad range of ~200 "client" proteins. (Taipale et al., 2010). In cancer cells, HSP90 acts as a molecular chaperone for numerous oncogenic proteins and is essential for their activity and stability, particularly for those that are activated by mutation(s) or overexpression (Taldone et al., 2019; Whitesell and Lindquist, 2005). Thus, the development of inhibitors of HSP90 is an attractive strategy for cancer treatment (Trepel et al., 2010). Moreover, inhibition of HSP90 shows promise for overcoming drug resistance that frequently limits successful cancer treatment, and for improving the efficacy of immunotherapy (Kryeziu et al., 2019).

Cutaneous squamous cell carcinomas (cSCC), which are most commonly caused by recreational or occupational exposure to solar ultraviolet radiation (UVR), represent some of the most frequently diagnosed keratinocyte skin cancers, and the most highly mutated human malignancies. Although surgical excision, radiotherapy, and chemotherapy are effective against primary tumors, mortality for metastatic cSCC is as high as 70% (Burton et al., 2016). Comprehensive characterization studies of the genomic changes that drive development of cSCC in both humans and mice have revealed mutations in numerous oncogenes and tumor suppressor genes (Chitsazzadeh et al., 2016; Knatko et al., 2017; South et al., 2014), implying that therapies that target individual oncoproteins are unlikely to succeed, and global approaches are needed for the prevention and treatment of these cancers. Topical treatment of the skin of mice with the HSP90 inhibitor 17-*N*-allylamino-17-demethoxygeldanamycin (17-AAG) prevents the development of UVR-induced SCC, and is accompanied by a decrease in UVR-induced hyperplasia of the skin, and lower levels of a number of HSP90 client proteins without any local or systemic toxicity (Singh et al., 2015). These preclinical observations suggest that HSP90 inhibitors could be developed as topical agents for prevention of cSCC.

Using click chemistry, we previously found that the mildly electrophilic compound sulfoxythiocarbamate alkyne (STCA) binds to cysteine residues of Kelch-like ECH associated protein 1 (Keap1) (Ahn et al., 2010) to activate transcription factor nuclear factor erythroid 2 p45-related factor 2 (Nrf2), which in turn regulates the expression of a network of genes encoding cytoprotective proteins (Cuadrado et al., 2019). Genetic or pharmacologic activation of Nrf2 is protective against UVR-induced skin damage in mice and humans (Dinkova-Kostova et al., 2008; Knatko et al., 2015; Talalay et al., 2007), and reduces the development of cSCC caused by chronic exposure to solar-simulated UVR in mice (Knatko et al., 2016; Knatko et al., 2015), suggesting that pharmacologic Nrf2 activators are good candidates for photoprotective agents. A mass spectrometry-based proteomic approach showed that in addition to Keap1, STCA also binds to HSP90 in cells (Ahn et al., 2010; Zhang et al., 2011) and covalently modifies cysteine residues of purified recombinant HSP90 *in vitro*, forming stable thiocarbamate adducts (Zhang et al., 2014). A cell-based screen of 19 sulfoxythiocarbamate derivatives identified compound S-4 (**Fig. 1A**) as an HSP90 inhibitor, which destabilizes multiple HSP90 client proteins and decreases proliferation of breast cancer cells (Zhang et al., 2014). Among the HSP90 clients downregulated by S-4 in these cells was HER2 (gene name *ERBB2*). Curiously, molecular similarities, including mutations in HER2, have been observed between cSCC and specific subtypes of breast cancer, suggesting common molecular vulnerabilities (Chitsazzadeh et al., 2016). In the present study we address the mechanism(s) by which S-4 compromises cell viability using early passages of patient-derived cSCC cells as a model system.

2. Materials and Methods

2.1. Materials

AUY922 (NVP-AUY922) was from ApexBio Technology. S-4 was synthesized as described (Zhang et al., 2014). The identity and purity (>94%) of S-4 were determined by ^{1}H- and ^{13}C-NMR spectroscopy and liquid chromatography-mass spectrometry (LC-MS). Spectra are shown in **Supplemental Fig. 1A**. For cell culture experiments, AUY922 was dissolved in DMSO and S-4 was dissolved in acetonitrile. Both solutions were then diluted (1:1000) in the cell culture medium. The concentration of solvent in the cell culture medium was maintained at 0.1%. All other general chemicals and reagents were of analytical grade and obtained from Sigma-Aldrich.

2.2. HSP90β expression and purification

A plasmid encoding human GST-HSP90β fusion protein (Zhang et al., 2014) was transformed into *E. coli* BL21 (DE3) codon plus cells. Cells were grown at 37°C in LB media until OD_{600} of 0.6-0.8, then induced at 37°C with isopropyl β-d-1-thiogalactopyranoside (IPTG, 1 mM) for 4 h. Cell pellets were collected by centrifugation and sonicated in PBS. Cell lysates were clarified by centrifugation at 17,700 x g. The supernatant was loaded onto Glutathione Sepharose 4 FF (GE healthcare) for affinity purification. Bound protein was cleaved by precision-protease at 4°C overnight, and HSP90β was collected in the flow-through fraction. Protein purity was confirmed following SDS-PAGE and Coomassie blue staining.

2.3. Cysteine modification of HSP90β by S-4

Purified HSP90β was dialyzed against 40 mM HEPES, pH 7.5, 20 mM KCl, and 1 mM tris(2-carboxyethyl)phosphine (TCEP). Dialysed Hsp90β (1 μM) was incubated with S-4

(15 μM) or DMSO (vehicle for S-4) in 50 μl of buffer (40 mM HEPES, pH 7.5, 20 mM KCl, 1 mM TCEP), at room temperature, for 2 h. The samples were then mixed with NuPAGE™ LDS Sample Buffer (Thermo Scientific), incubated at room temperature for 30 min, and gel-purified using NuPAGE™ 4-12% Bis-Tris gel and NuPAGE™ MOPS SDS Running Buffer (Thermo Scientific). The gel was stained with InstantBlue™ (Expedeon) and the Hsp90β band was excised, reduced with TCEP, alkylated with 2-iodoacetamide (IAA), in-gel digested with trypsin, and subjected to analysis by liquid chromatography-mass spectrometry (LC-MS) on an Orbitrap Velos equipped with Easy spray source and Ultimate 3000 UPLC.

2.4. Cell culture

The establishment of the human cutaneous squamous cell carcinoma cell lines SCC IC1 and SCC IC12 has been previously described (Proby et al., 2000). Cell lines were cultured in RM+ media with the following composition: a mixture of DMEM:Ham's F12 (3:1) (Thermo Scientific) media supplemented with 10% fetal bovine serum (FBS, Thermo Scientific), 0.4 μg/ml hydrocortisone (Sigma), 5 μg/ml insulin (Sigma), 10 ng/ml epidermal growth factor (EGF, Serotec), 5 μg/ml transferrin (Sigma), 8.4 ng/ml cholera toxin (Sigma) and 13 ng/ml liothyronine (Sigma). Normal Human Keratinocyte (NHK) cells were isolated from breast or abdominal skin of human subjects after informed consent, initially grown in the presence of a mitotically inactivated NIH3T3 fibroblast feeder layer as described (Rheinwald, 1980), and cryopreserved. Frozen NHK cells were rapidly thawed in a 37°C water bath and cultured overnight in RM- (same composition as RM+, but without EGF) media. On the next day, the media was replaced with RM+ media. Cells were maintained in a humidified atmosphere at 37°C and 5% CO_2.

2.5. ATP-binding assay

SCC IC1 cells (0.5×10^6) growing in 6-cm dishes were treated for 24 h with either 0.1% (v/v) acetonitrile (vehicle for S-4), 7.5 μM S-4, 0.1% DMSO (vehicle for AUY922) or 0.1 μM AUY922. Using a scraper, cells were collected into 300 μl of lysis buffer (10 mM Tris pH 7.5, 150 mM NaCl, 0.25% NP40, with one protease inhibitor tablet (Roche) per 10.0 ml of buffer), and the cell suspension was frozen, thawed, and lysed for 30 min at 4°C. ATP-agarose beads (Jena Bioscience, AC-101S) were washed with incubation buffer (10 mM Tris pH 7.5, 150 mM NaCl, 20 mM MgCl2, 0.05% NP40, 1 mM DTT). The beads suspension (30 μl) was mixed with 200 μg of protein in a final volume of 1.25 ml of buffer, and incubated rotating overnight at 4°C. The beads were then collected by centrifugation and washed three times with incubation buffer. Following addition of 10 μl of sodium dodecyl sulfate (SDS) loading buffer and 40 μl of incubation buffer, the samples were heated at 100°C for 5 min. The beads were pelleted by centrifugation, and the supernatants were collected and subjected to immunoblotting analysis.

2.6. Immunoblotting

Cells growing on 6-well plates were lysed in 150 μl of non-reducing sample buffer (50 mM Tris-HCl pH 6.8, 2% (w/v) sodium dodecyl sulfate (SDS), 10% (v/v) glycerol, and 0.02% (w/v) Bromophenol blue). Whole-cell lysates were then collected in Eppendorf tubes, boiled at 100°C for 5 min, and sonicated using Vibra-Cell ultrasonic processor (Sonic) for 20 sec at 20% amplitude. The BCA assay (Thermo) was used to determine protein concentrations. 2-Mercaptoethanol (Sigma) was added to a final concentration of 6% (v/v). Proteins were resolved by SDS/PAGE, and then transferred to 0.45 μm nitrocellulose (NC) membranes (Thermo Scientific). Solutions of primary antibodies were prepared in 3% BSA (antibodies against phospho-proteins) or 5% milk (all other) in PBST. The following antibodies and dilutions were used: mouse monoclonal anti-HSP70, 1:1000, StressMarq,

SMC-100B; rabbit monoclonal anti-phospho-HSF1 (Ser326), 1:5000, Abcam, ab76076; rabbit monoclonal anti-Hsp90β, 1:5000, Abcam, ab203085; rabbit polyclonal anti-HER2, 1:500, Millipore, 06-562; rabbit monoclonal anti-Bcl-2, 1:1000, CST, 2870; rabbit monoclonal anti-cytochrome c, 1:1000, CST, 11940T; rabbit monoclonal anti-CDK4, 1:1000, CST, 12790T; rabbit monoclonal anti-cyclin D1, 1:1000, CST, 2978T; rabbit polyclonal anti-phospho-Rb (Ser795), 1:1000, CST, 9301T; rabbit monoclonal anti-phospho-Rb (Ser608), 1:1000, CST, 8147T; rabbit polyclonal anti-GAPDH, 1:5,000, Sigma, G9545; rabbit polyclonal anti-VDAC-1, 1:10000, Abcam, ab154856; mouse monoclonal anti-β-actin, 1:20000, Sigma, A5441. Blocked NC membranes were incubated with the primary antibody solutions in 50-ml tubes at 4°C overnight, with continuous rotation. After this, the NC membranes were washed and incubated with the corresponding secondary antibodies (horseradish peroxidase (HRP)-conjugated goat anti-rabbit or goat anti-mouse antibodies, 1:5000, BioRad). Thermo Scientific SuperSignal West Dura Extended Duration Substrate was used for signal development. For the experiment shown in Fig. 2, IRDye fluorescent dyes conjugated to secondary antibodies (GAM/GAR-800CW, 1:15000, LI-COR) were used. Image capture and analysis were done using the Odyssey® CLx image system and Image Studio software (LI-COR).

2.7. Cell viability assay

Cells (5 x 10^3 per well) were seeded in white flat-bottomed 96-well plates (Nunc). On the next day, cells were treated with 0.1% (v/v) acetonitrile (vehicle control) or increasing concentrations of S-4 for 24, 48 or 72 h. Four h before the end of each treatment, 10 µl of alamar blue dye solution (AbdSerotec) was added to the cell culture media (100 µl) within each well, and the plates were returned to the incubator. After 4 h, the fluorescence of the reduced probe was determined (ex. 560 nm/ em. 590 nm, SpectraMax M2, Molecular

Devices), from which the cell viability was calculated. For both cell types, the experiment was done on two separate occasions, each time using 8 replicate wells of cells.

2.8. Cell proliferation assay

Cell proliferation was followed for 3 days using the CellTrace™ CFSE (carboxyfluorescein diacetate succinimidyl ester, Thermo Scientific). Briefly, cells were labelled with 2.5 μM CFSE according to the manufacturer's protocol, and seeded at a density of 2.5×10^5 per well in 6-well plates. On the next day, cells were treated with 0.1% (v/v) acetonitrile (vehicle control) or increasing concentrations of S-4. At the indicated time points, the cells were collected and analyzed using BD LSRFortessa™ cell analyzer with 488 nm excitation and emission filters appropriate for fluorescein to measure CFSE fluorescence. This experiment was done twice.

2.9. Cell cycle analysis

Cells were seeded at a density of 2.5×10^5 per well in 6-well plates. On the next day, cells were treated with 0.1% (v/v) acetonitrile or increasing concentration of S-4 for the indicated time periods. After treatment, the cells were collected and fixed with 70% ethanol at -20℃ overnight. Cells were then washed with PBS and stained with PI (40 μg/ml) in the presence of RNase A (100 μg/ml) at 37°C for 30 min in the dark. The DNA content was detected using BD LSRFortessa™ cell analyzer. The data were analyzed in FlowJo. The experiment was done on three separate occasions.

2.10. Data analysis

All quantitative data are represented graphically as mean values ± 1 standard deviation (S.D.). The differences between groups were determined by Student's t-test.

3. Results

3.1. S-4 upregulates HSP70 in cSCC cells

The cell line SCC IC1 was originally isolated from the primary site of a moderately differentiated metastatic squamous cell carcinoma that had been formed on the right temple of an immunocompetent 77-year-old male patient. SCC IC1 cells have well characterized mutational spectrum comprised of multiple UV radiation signature mutations, including mutations in *TP53* (H179Y, R248W), *NOTCH1* (N1809H), *NOTCH2* (P1913S) and *ERBB2* (E1068K) (South et al., 2014). For some experiments, we also used SCC IC12 cells isolated from a moderately/poorly differentiated squamous cell carcinoma that had been formed on the left calf of an immunocompetent 87-year-old female patient.

Monitoring the activation of transcription factor heat shock factor 1 (HSF1), the master regulator of the heat shock response, by the enhanced expression of its downstream target proteins such as heat shock protein 70 (HSP70), represents a mechanistically unbiased approach to screen individual compounds and chemical libraries for identification of HSP90 inhibitors (Santagata et al., 2012). Induction of HSP70 correlates with degradation of HSP90 client protein in peripheral blood lymphocytes and xenograft tumors (Mehta et al., 2011), and is used as a pharmacodynamic marker in clinical trials with HSP90 inhibitors (Shimomura et al., 2019). Therefore, to begin evaluating the ability of S-4 to inhibit HSP90 in SCC IC1 cells, we used induction of HSP70 as the first endpoint. The concentration range of S-4 was chosen based on a cell viability assay, which showed 20- and 50% loss of viability of SCC IC1 cells at 72 h post-exposure to 5- and 7.5 μM S-4, respectively (**Fig. 1B**). Importantly, these concentrations of S-4 were less toxic to cultured normal human keratinocytes (NHK) cells, and >90- and 80% of them were viable 72 h after 5- and 7.5 μM S-4 treatment, respectively (**Fig. 1C**). We found that the levels of HSP70 increased in a concentration-dependent

manner 24 h after exposure of SCC IC1 cells to S-4 (**Fig. 1D**). Similar results were obtained in SCC IC12 cells (**Supplemental Fig. 2A**). A time-course experiment following exposure of SCC IC1 cells to 7.5 μM S-4 further showed that induction of HSP70 was time-dependent, and among the time points tested, was maximal at the 24-h time point (**Fig. 1E**). The induction of HSP70 was preceded by a transient increase in the levels of phosphorylated HSF1 at S326, a hallmark of HSF1 activation (**Fig. 1E**). These results are in close agreement with the ability of S-4, and other structurally related sulfoxythiocarbamates, to induce HSP70 in breast cancer cell lines (Zhang et al., 2014).

3.2. S-4 binds to cysteine residues of HSP90β

Although induction of HSP70 can be a consequence of HSP90 inhibition by compounds that bind to the N-terminus of the chaperone, it can also occur independently of HSP90. Wang et al. (Wang et al., 2017) have reported that the cellular phenotypes resulting from treatments with N-terminal HSP90 inhibitors (e.g. AUY922 or 17-AAG) differ from the phenotype caused by a knockdown of HSP90, whereas those consequent to treatments with C-terminal HSP90 inhibitors, phenocopy HSP90-deficient cells. We have previously shown that STCA forms covalent thiocarbamate adducts with cysteine residues in the middle domain of HSP90 (Zhang et al., 2014). To test the possibility that S-4 acts by a similar mechanism, we produced recombinant purified human HSP90β and incubated it with S-4 or its vehicle control for 2 h. Following gel purification and in-gel tryptic digestion of the modified protein, the resulting peptides were subjected to mass spectrometry analysis. Five peptides were identified in the S-4-treated sample, which were absent in the vehicle-treated sample (**Table S1**), collectively revealing that S-4 formed covalent adducts with C521, and C589/C590 of HSP90β.

Notably, C521, C589, and C590 are located in the middle domain of HSP90, suggesting that their modification may interfere with the ability of HSP90 to bind its co-chaperones and/or client proteins, but not with its ATP-binding ability. It was still theoretically possible however that S-4 binds non-covalently to the N-terminal domain of HSP90. To test for this possibility, we performed an ATP-agarose pull-down of lysates from SCC IC1 cells that had been treated with S-4 or its vehicle control. As expected, treatment with the N-terminal inhibitor AUY922, which was used as positive control, abolished binding of HSP90 to ATP (**Fig. 2**). By contrast, ATP binding of HSP90 was not altered by S-4 (**Fig. 2**). Because ATP binds to the N-terminal domain of HSP90, this result further confirms that the mode of action of S-4 is distinct from that of N-terminal inhibitors.

3.3. S-4 destabilizes the HSP90 client proteins HER2 and Bcl-2

Next, we tested the functional consequences of S-4 binding to HSP90. SCC IC1 cells carry mutant HER2, a tyrosine kinase oncoprotein, which has been shown to interact strongly with HSP90, emphasizing the importance of the chaperone for HER2 stability (Taipale et al., 2012). Consistent with HSP90 inhibition, exposure of SCC IC1 cells to S-4 for 24 h led to a concentration-dependent decrease in the levels of immunologically detectable HER2 (**Fig. 3A**). A time-course experiment further revealed a clear decrease of HER2 at the 8- and the 24-h time-points (**Fig. 3B**). A concentration-dependent decrease in the levels of HER2 after exposure to S-4 was similarly observed in SCC IC12 cells (**Supplemental Fig. 2B**). Pharmacological inhibition of HSP90 has been shown to cause downregulation of another HSP90 client, Bcl-2 (Gallerne et al., 2013), a protein of critical importance for the integrity of the mitochondrial membrane (Harris and Thompson, 2000). In agreement with the dependence of Bcl-2 on HSP90 and HSP90 inhibition by S-4, we found that the levels of Bcl-

2 were reduced in cells treated with 7.5 μM S-4, especially at the early (2- and 4-h) time points (**Fig. 3C**).

3.4. S-4 promotes cytochrome c release

Bcl-2 is an anti-apoptotic protein, which together with Bcl-xL, inhibits Bax-mediated apoptosis, promoting cell survival (Zha et al., 1996). To further explore the functional consequences of S-4 treatment, we considered the possibility that, by destabilizing Bcl-2, S-4 may release its inhibitory effect on Bax. This would allow Bax to form pores on the mitochondrial membrane, in turn leading to cytochome c release and activation of apoptosis. A sub-cellular fractionation experiment showed that exposure to S-4 led to a concentration-dependent cytochrome c release in the cytoplasm (**Fig. 3D**), suggesting induction of apoptosis via the intrinsic apoptotic pathway.

3.5. S-4 causes cell cycle arrest

Treatment with S-4 for 24 h caused inhibition in cell proliferation in a concentration-dependent manner (**Fig. 4A**), and this effect was even more pronounced at 48 h post-treatment in both SCC IC1 (**Fig. 4B**) and SCC IC12 (**Supplemental Fig. 3A**) cells. One possible explanation was that those cells that survived apoptosis were undergoing cell cycle arrest. To address this possibility, cell cycle analysis was performed. This analysis showed that S-4 caused a concentration-dependent arrest at the G0/1 phase of the cell cycle at 24 h following exposure to S-4 (**Fig. 4C**). Overall, from three independent experiments, at 24 h, compared to vehicle-treatment, the cell population in G0/1 was increased by 2.1-fold ($P = 0.05$) and 2.8-fold ($P = 0.036$) after treatment with 5- or 7.5 μM S-4, respectively (**Fig. 4D**). Similar results were obtained in SCC IC12 cells (**Supplemental Fig. 3B**).

During early G1, the transcription factor E2F is inhibited by interaction with retinoblastoma susceptibility protein Rb (**Fig. 5A**). Activation of the cyclin D-CDK4/6 protein complex results in the phosphorylation of Rb at multiple sites, which then releases E2F, in turn activating the transcription of genes that allow G1-S phase progression (Knudsen and Knudsen, 2008). Importantly, E2F was identified as a key transcriptional driver in the early stages of the development of cSCC in both humans and mice (Chitsazzadeh et al., 2016). Both CDK4 and cyclin D1 are HSP90 client proteins (Vaughan et al., 2006). Consistent with HSP90 inhibition, the levels of CDK4 and cyclin D1 decreased in a time-dependent manner in S-4-treated cells (**Fig. 5B**). In agreement with the decreased levels of CDK4 and cyclin D1, the levels of phosphorylated Rb at S608 and S795 were also lower in S-4-treated cells (**Fig. 5B**). Together, these experiments suggest that S-4 causes destabilization of cyclin D1 and CDK4, consequently decreasing the phosphorylation of Rb and promoting G1-S cell cycle arrest.

4. Discussion

A large number of HSP90 inhibitors have been developed, and several have been tested in clinical trials (Jhaveri et al., 2012). Most have demonstrated limited clinical efficacy and unacceptable adverse events, such as ocular toxicities that are likely caused by photoreceptor cell death consequent to sustained HSP90 inhibition in the retina (Aguila et al., 2014; Zhou et al., 2013). A recent clinical trial in patients with advanced solid tumors with the orally-administered pyrazolo[3,4- b]pyridine derivative TAS-116 has identified specific dosing regimens with promising safety and efficacy profiles, forming the basis for the current testing of this HSP90 inhibitor in patients with non-small cell lung cancer, gastrointestinal stromal tumors, and HER2-positive breast cancer (Shimomura et al., 2019).

Following from our previous findings that sulfoxythiocarbamate derivatives induce transcription factor Nrf2 (Ahn et al., 2010) and inhibit HSP90 and the proliferation of breast cancer cells (Zhang et al., 2014), in this study, we investigated the mechanism(s) by which the sulfoxythiocarbamate S-4 compromises the viability of cancer cells using two patient-derived primary cSCC cell lines. Based on the current results, we propose a model, which is summarized in **Fig. 6**. S-4 inhibits HSP90, causing depletion of its client proteins, including Bcl-2, cyclin D1 and CDK4. Depletion of Bcl-2 allows Bax to form pores on the mitochondrial membrane, triggering cytochrome c release. Depletion of the HSP90 clients cyclin D1 and CDK4 by S-4 does not allow phosphorylation of Rb and the release of E2F and prevents G1-S cell cycle progression. Together, these processes lead to compromised cell viability.

This model is based on our new findings that treatment with S-4 decreases the levels of Bcl-2, cyclin D1 and CDK4, all of which are well-established HSP90 clients, and the known functions of these proteins in apoptosis and the cell cycle. It should be noted however that S-4 is not a selective inhibitor of HSP90, and other potential mechanisms could also be contributing to the observed effects. By virtue of its sulfhydryl reactivity, S-4 may also bind to other cellular proteins, similarly to the closely related sulfoxythiocarbamate alkyne (STCA) (Ahn et al., 2010). Indeed, S-4 activates transcription factor Nrf2, as evidenced by the increase in the levels of the classical Nrf2-target protein, NAD(P)H:quinone oxidoreductase 1 (NQO1) (Zhang et al., 2014). Importantly, Nrf2 activation by compounds of this type requires lower concentrations than the concentrations that inhibit HSP90/induce HSP70 (Zhang et al., 2011) as Keap1 is endowed with highly reactive cysteine sensors (Dinkova-Kostova et al., 2002). Pharmacologic Nrf2 activation results in comprehensive multi-organ cytoprotection, including protection of the retina (Gao and Talalay, 2004; Pitha-Rowe et al., 2009; Tanito et al., 2005), and therefore could counteract some of the negative

consequences of HSP90 inhibition. Thus, the ability of S-4 to both activate Nrf2 and inhibit HSP90 offers the advantage of protecting normal cells and tissues, whilst causing cell cycle arrest of cancer cells, which are much more reliant on HSP90 than normal cells for growth and survival.

References

Aguila, M., Bevilacqua, D., McCulley, C., Schwarz, N., Athanasiou, D., Kanuga, N., Novoselov, S.S., Lange, C.A., Ali, R.R., Bainbridge, J.W., Gias, C., Coffey, P.J., Garriga, P., Cheetham, M.E., 2014. Hsp90 inhibition protects against inherited retinal degeneration. Hum Mol Genet 23, 2164-2175.

Ahn, Y.H., Hwang, Y., Liu, H., Wang, X.J., Zhang, Y., Stephenson, K.K., Boronina, T.N., Cole, R.N., Dinkova-Kostova, A.T., Talalay, P., Cole, P.A., 2010. Electrophilic tuning of the chemoprotective natural product sulforaphane. Proc Natl Acad Sci U S A 107, 9590-9595.

Burton, K.A., Ashack, K.A., Khachemoune, A., 2016. Cutaneous Squamous Cell Carcinoma: A Review of High-Risk and Metastatic Disease. Am J Clin Dermatol 17, 491-508.

Chitsazzadeh, V., Coarfa, C., Drummond, J.A., Nguyen, T., Joseph, A., Chilukuri, S., Charpiot, E., Adelmann, C.H., Ching, G., Nguyen, T.N., Nicholas, C., Thomas, V.D., Migden, M., MacFarlane, D., Thompson, E., Shen, J., Takata, Y., McNiece, K., Polansky, M.A., Abbas, H.A., Rajapakshe, K., Gower, A., Spira, A., Covington, K.R., Xiao, W., Gunaratne, P., Pickering, C., Frederick, M., Myers, J.N., Shen, L., Yao, H., Su, X., Rapini, R.P., Wheeler, D.A., Hawk, E.T., Flores, E.R., Tsai, K.Y., 2016. Cross-species identification of genomic drivers of squamous cell carcinoma development across preneoplastic intermediates. Nature communications 7, 12601.

Cuadrado, A., Rojo, A.I., Wells, G., Hayes, J.D., Cousin, S.P., Rumsey, W.L., Attucks, O.C., Franklin, S., Levonen, A.L., Kensler, T.W., Dinkova-Kostova, A.T., 2019. Therapeutic targeting of the NRF2 and KEAP1 partnership in chronic diseases. Nature reviews. Drug discovery 18, 295-317.

Dinkova-Kostova, A.T., Holtzclaw, W.D., Cole, R.N., Itoh, K., Wakabayashi, N., Katoh, Y., Yamamoto, M., Talalay, P., 2002. Direct evidence that sulfhydryl groups of Keap1 are the sensors regulating induction of phase 2 enzymes that protect against carcinogens and oxidants. Proc Natl Acad Sci U S A 99, 11908-11913.

Dinkova-Kostova, A.T., Jenkins, S.N., Wehage, S.L., Huso, D.L., Benedict, A.L., Stephenson, K.K., Fahey, J.W., Liu, H., Liby, K.T., Honda, T., Gribble, G.W., Sporn, M.B., Talalay, P., 2008. A dicyanotriterpenoid induces cytoprotective enzymes and reduces multiplicity of skin tumors in UV-irradiated mice. Biochem Biophys Res Commun 367, 859-865.

Gallerne, C., Prola, A., Lemaire, C., 2013. Hsp90 inhibition by PU-H71 induces apoptosis through endoplasmic reticulum stress and mitochondrial pathway in cancer cells and overcomes the resistance conferred by Bcl-2. Biochim Biophys Acta 1833, 1356-1366.

Gao, X., Talalay, P., 2004. Induction of phase 2 genes by sulforaphane protects retinal pigment epithelial cells against photooxidative damage. Proc Natl Acad Sci U S A 101, 10446-10451.

Harris, M.H., Thompson, C.B., 2000. The role of the Bcl-2 family in the regulation of outer mitochondrial membrane permeability. Cell Death Differ 7, 1182-1191.

Jhaveri, K., Taldone, T., Modi, S., Chiosis, G., 2012. Advances in the clinical development of heat shock protein 90 (Hsp90) inhibitors in cancers. Biochim Biophys Acta 1823, 742-755.

Knatko, E.V., Higgins, M., Fahey, J.W., Dinkova-Kostova, A.T., 2016. Loss of Nrf2 abrogates the protective effect of Keap1 downregulation in a preclinical model of cutaneous squamous cell carcinoma. Scientific reports 6, 25804.

Knatko, E.V., Ibbotson, S.H., Zhang, Y., Higgins, M., Fahey, J.W., Talalay, P., Dawe, R.S., Ferguson, J., Huang, J.T., Clarke, R., Zheng, S., Saito, A., Kalra, S., Benedict, A.L., Honda, T., Proby, C.M., Dinkova-Kostova, A.T., 2015. Nrf2 Activation Protects against Solar-

Simulated Ultraviolet Radiation in Mice and Humans. Cancer Prev Res (Phila) 8, 475-486.
Knatko, E.V., Praslicka, B., Higgins, M., Evans, A., Purdie, K.J., Harwood, C.A., Proby, C.M., Ooi, A., Dinkova-Kostova, A.T., 2017. Whole-Exome Sequencing Validates a Preclinical Mouse Model for the Prevention and Treatment of Cutaneous Squamous Cell Carcinoma. Cancer Prev Res (Phila) 10, 67-75.
Knudsen, E.S., Knudsen, K.E., 2008. Tailoring to RB: tumour suppressor status and therapeutic response. Nat Rev Cancer 8, 714-724.
Kryeziu, K., Bruun, J., Guren, T.K., Sveen, A., Lothe, R.A., 2019. Combination therapies with HSP90 inhibitors against colorectal cancer. Biochim Biophys Acta Rev Cancer 1871, 240-247.
Mehta, P.P., Whalen, P., Baxi, S.M., Kung, P.P., Yamazaki, S., Yin, M.J., 2011. Effective targeting of triple-negative breast cancer cells by PF-4942847, a novel oral inhibitor of Hsp 90. Clin Cancer Res 17, 5432-5442.
Pitha-Rowe, I., Liby, K., Royce, D., Sporn, M., 2009. Synthetic triterpenoids attenuate cytotoxic retinal injury: cross-talk between Nrf2 and PI3K/AKT signaling through inhibition of the lipid phosphatase PTEN. Invest Ophthalmol Vis Sci 50, 5339-5347.
Proby, C.M., Purdie, K.J., Sexton, C.J., Purkis, P., Navsaria, H.A., Stables, J.N., Leigh, I.M., 2000. Spontaneous keratinocyte cell lines representing early and advanced stages of malignant transformation of the epidermis. Exp Dermatol 9, 104-117.
Rheinwald, J.G., 1980. Serial cultivation of normal human epidermal keratinocytes. Methods Cell Biol 21A, 229-254.
Santagata, S., Xu, Y.M., Wijeratne, E.M., Kontnik, R., Rooney, C., Perley, C.C., Kwon, H., Clardy, J., Kesari, S., Whitesell, L., Lindquist, S., Gunatilaka, A.A., 2012. Using the heat-shock response to discover anticancer compounds that target protein homeostasis. ACS Chem Biol 7, 340-349.
Shimomura, A., Yamamoto, N., Kondo, S., Fujiwara, Y., Suzuki, S., Yanagitani, N., Horiike, A., Kitazono, S., Ohyanagi, F., Doi, T., Kuboki, Y., Kawazoe, A., Shitara, K., Ohno, I., Banerji, U., Sundar, R., Ohkubo, S., Calleja, E.M., Nishio, M., 2019. First-in-Human Phase I Study of an Oral HSP90 Inhibitor, TAS-116, in Patients with Advanced Solid Tumors. Mol Cancer Ther 18, 531-540.
Singh, A., Singh, A., Sand, J.M., Bauer, S.J., Hafeez, B.B., Meske, L., Verma, A.K., 2015. Topically applied Hsp90 inhibitor 17AAG inhibits UVR-induced cutaneous squamous cell carcinomas. J Invest Dermatol 135, 1098-1107.
South, A.P., Purdie, K.J., Watt, S.A., Haldenby, S., den Breems, N.Y., Dimon, M., Arron, S.T., Kluk, M.J., Aster, J.C., McHugh, A., Xue, D.J., Dayal, J.H., Robinson, K.S., Rizvi, S.M., Proby, C.M., Harwood, C.A., Leigh, I.M., 2014. NOTCH1 Mutations Occur Early during Cutaneous Squamous Cell Carcinogenesis. J Invest Dermatol 134, 2630-2638.
Taipale, M., Jarosz, D.F., Lindquist, S., 2010. HSP90 at the hub of protein homeostasis: emerging mechanistic insights. Nat Rev Mol Cell Biol 11, 515-528.
Taipale, M., Krykbaeva, I., Koeva, M., Kayatekin, C., Westover, K.D., Karras, G.I., Lindquist, S., 2012. Quantitative analysis of HSP90-client interactions reveals principles of substrate recognition. Cell 150, 987-1001.
Talalay, P., Fahey, J.W., Healy, Z.R., Wehage, S.L., Benedict, A.L., Min, C., Dinkova-Kostova, A.T., 2007. Sulforaphane mobilizes cellular defenses that protect skin against damage by UV radiation. Proc Natl Acad Sci U S A 104, 17500-17505.
Taldone, T., Wang, T., Rodina, A., Pillarsetty, N.V.K., Digwal, C.S., Sharma, S., Yan, P., Joshi, S., Pagare, P.P., Bolaender, A., Roboz, G.J., Guzman, M.L., Chiosis, G., 2019. A Chemical

Biology Approach to the Chaperome in Cancer-HSP90 and Beyond. Cold Spring Harbor perspectives in biology.
Tanito, M., Masutani, H., Kim, Y.C., Nishikawa, M., Ohira, A., Yodoi, J., 2005. Sulforaphane induces thioredoxin through the antioxidant-responsive element and attenuates retinal light damage in mice. Invest Ophthalmol Vis Sci 46, 979-987.
Trepel, J., Mollapour, M., Giaccone, G., Neckers, L., 2010. Targeting the dynamic HSP90 complex in cancer. Nat Rev Cancer 10, 537-549.
Vaughan, C.K., Gohlke, U., Sobott, F., Good, V.M., Ali, M.M., Prodromou, C., Robinson, C.V., Saibil, H.R., Pearl, L.H., 2006. Structure of an Hsp90-Cdc37-Cdk4 complex. Mol Cell 23, 697-707.
Wang, Y., Koay, Y.C., McAlpine, S.R., 2017. Redefining the Phenotype of Heat Shock Protein 90 (Hsp90) Inhibitors. Chemistry 23, 2010-2013.
Whitesell, L., Lindquist, S.L., 2005. HSP90 and the chaperoning of cancer. Nat Rev Cancer 5, 761-772.
Zha, J., Harada, H., Yang, E., Jockel, J., Korsmeyer, S.J., 1996. Serine phosphorylation of death agonist BAD in response to survival factor results in binding to 14-3-3 not BCL-X(L). Cell 87, 619-628.
Zhang, Y., Ahn, Y.H., Benjamin, I.J., Honda, T., Hicks, R.J., Calabrese, V., Cole, P.A., Dinkova-Kostova, A.T., 2011. HSF1-dependent upregulation of Hsp70 by sulfhydryl-reactive inducers of the KEAP1/NRF2/ARE pathway. Chem Biol 18, 1355-1361.
Zhang, Y., Dayalan Naidu, S., Samarasinghe, K., Van Hecke, G.C., Pheely, A., Boronina, T.N., Cole, R.N., Benjamin, I.J., Cole, P.A., Ahn, Y.H., Dinkova-Kostova, A.T., 2014. Sulphoxythiocarbamates modify cysteine residues in HSP90 causing degradation of client proteins and inhibition of cancer cell proliferation. Br J Cancer 110, 71-82.
Zhou, D., Liu, Y., Ye, J., Ying, W., Ogawa, L.S., Inoue, T., Tatsuta, N., Wada, Y., Koya, K., Huang, Q., Bates, R.C., Sonderfan, A.J., 2013. A rat retinal damage model predicts for potential clinical visual disturbances induced by Hsp90 inhibitors. Toxicol Appl Pharmacol 273, 401-409.

Acknowledgments

We thank Wenzhang Chen and the FingerPrints Proteomics Facility of the University of Dundee School of Life Sciences for mass spectrometry analysis. We acknowledge with gratitude the financial support of the Biotechnology and Biological Sciences Research Council (BBSRC, Project Grant BB/J007498/1) and Cancer Research UK (C20953/A18644).

Author Contributions

Conceptualization, A.T.D-K. and Y.A.; Reagents, G.C.V. and C.M.P.; Investigation, Y.Z.; Data Analysis, Y.Z. and A.T.D-K.; Writing – Original Draft, Y.Z. and A.T.D-K.; Writing – Review & Editing, Y.Z., Y.A., C.M.P. and A.T.D-K.; Funding Acquisition, A.T.D-K.; Supervision, A.T.D-K. All authors read and approved the final manuscript.

Competing interests

A.T.D-K. is a member of the Scientific Advisory Board of Evgen Pharma, and a consultant for Aclipse Therapeutics and Vividion Therapeutics.

Figure Legends

Fig. 1. S-4 induces HSP70. (**A**) Chemical structure of S-4. (**B,C**) Viability of SCC IC1 cells (**B**) and normal human keratinocyte (NHK) cells (**C**) that had been left untreated, or had been treated with vehicle (0.1% acetonitrile) or S-4 (2.5-, 5- or 7.5 μM) for the indicated periods of time. *, $p<0.05$ relative to vehicle-treated cells (Student's t-test). (**D**) Immunoblotting analysis for HSP70 in SCC IC1 cells that had been exposed to increasing concentrations of S-4 for 24 h. GAPDH served as the loading control. (**E**) Immunoblotting analysis for HSP70 and phosphorylated HSF1 (at S326) in cells that had been exposed to S-4 (7.5 μM) for increasing periods of time. β-actin served as the loading control. Results are representative of 2 independent experiments.

Fig. 2. S-4 does not interfere with the ability of HSP90β to bind ATP. SCC IC1 cells were exposed for 24 h to acetonitrile (0.1%), S-4 (7.5 μM in 0.1% acetonitrile), DMSO (0.1%), or AUY922 (0.1 μM in 0.1% DMSO), lysed and subjected to ATP pull-down using ATP-agarose beads. The levels of HSP90β, HSP70 and β-actin were determined by immunoblotting. Results are representative of 2 independent experiments.

Fig. 3. S-4 destabilizes the HSP90 client proteins HER2 and Bcl-2. (**A,B**) Immunoblotting analysis for HER2 in cells that had been exposed to increasing concentrations of S-4 for 24 h (**A**) or to 7.5 μM of S-4 for the indicated periods of time (**B**). (**C**) Immunoblotting analysis for Bcl-2 in cells that had been exposed to S-4 (7.5 μM) for the indicated periods of time. The band in the red square corresponds to Bcl-2; the faster-migrating band is a non-specific protein. (**D**) Immunoblotting analysis for cytochrome c in the cytoplasmic fraction of cells that had been exposed to increasing concentrations of S-4 for 8 h. β-actin served as the loading control. The absence of detectable VDAC-1 served as evidence for the absence of

mitochondrial contamination in the purified cytoplasmic fraction. In all experiments, acetonitrile (0.1%) served as the vehicle control and β-actin served as the loading control. Immunoblots are representative of 2 independent experiments.

Fig. 4. S-4 causes cell cycle arrest. (**A, B**) Flow cytometry analysis of cells that had been labeled with CFSE and treated with vehicle (0.1% acetonitrile) or increasing concentrations of S-4 for either 24- (**A**) or 48- (**B**) h. (**C**) Cell cycle analysis of cells that had been left untreated, or treated with vehicle (0.1% acetonitrile) or S-4 (5- or 7.5 μM) for the indicated periods of time. Results are representative of 3 independent experiments. (**D**) Combined results of cell cycle analysis following treatment with vehicle (0.1% acetonitrile) or S-4 (5- or 7.5 μM) for 24 h. P = 0.05 for cells treated with 5 μM S-4 compared to vehicle-treated cells; P = 0.036 for cells treated with 7.5 μM S-4 compared to vehicle-treated cells (Student's t-test).

Fig. 5. S-4 causes depletion of the HSP90 client proteins CDK4 and cyclin D1, and inhibition of phosphorylation of the Rb protein. (**A**) The cyclin D-CDK4/6 protein complex phosphorylates Rb, which releases E2F to activate the transcription of genes that allow G1-S phase progression. (**B**) Immunoblotting analysis for CDK4, cyclin D1, and Rb protein phosphorylated at S608 and S795 in cells that had been exposed to S-4 (7.5 μM) for the indicated periods of time. β-actin served as the loading control. In **B**, CDK4 was detected on the lower section of the same membrane shown in Fig. 1E, whereas HSP70 was detected using the membrane upper section; Cyclin D1 was detected on the lower section of the same membrane shown in Fig. 1E, whereas pHSF1(S326) was detected using the membrane upper section; pRb(S795) was detected on the lower section of the same membrane shown in Fig. 3B, whereas HER2 was detected on the membrane upper section, and thus each of these two

blots share the same β-actin loading control. Immunoblots are representative of 2 independent experiments.

Fig. 6. Proposed model for the mechanism by which S-4 decreases the viability of SCC IC1 cells. S-4 inhibits HSP90, causing depletion of its client proteins, including Bcl-2, cyclin D1 and CDK4. The decrease in Bcl-2 allows Bax to form pores on the mitochondrial membrane, triggering cytochrome c release, suggesting apoptosis. Depletion of the HSP90 clients cyclin D1 and CDK4 prevents phosphorylation of Rb and the release of E2F, inhibiting G1-S cell cycle progression.

Figure 1

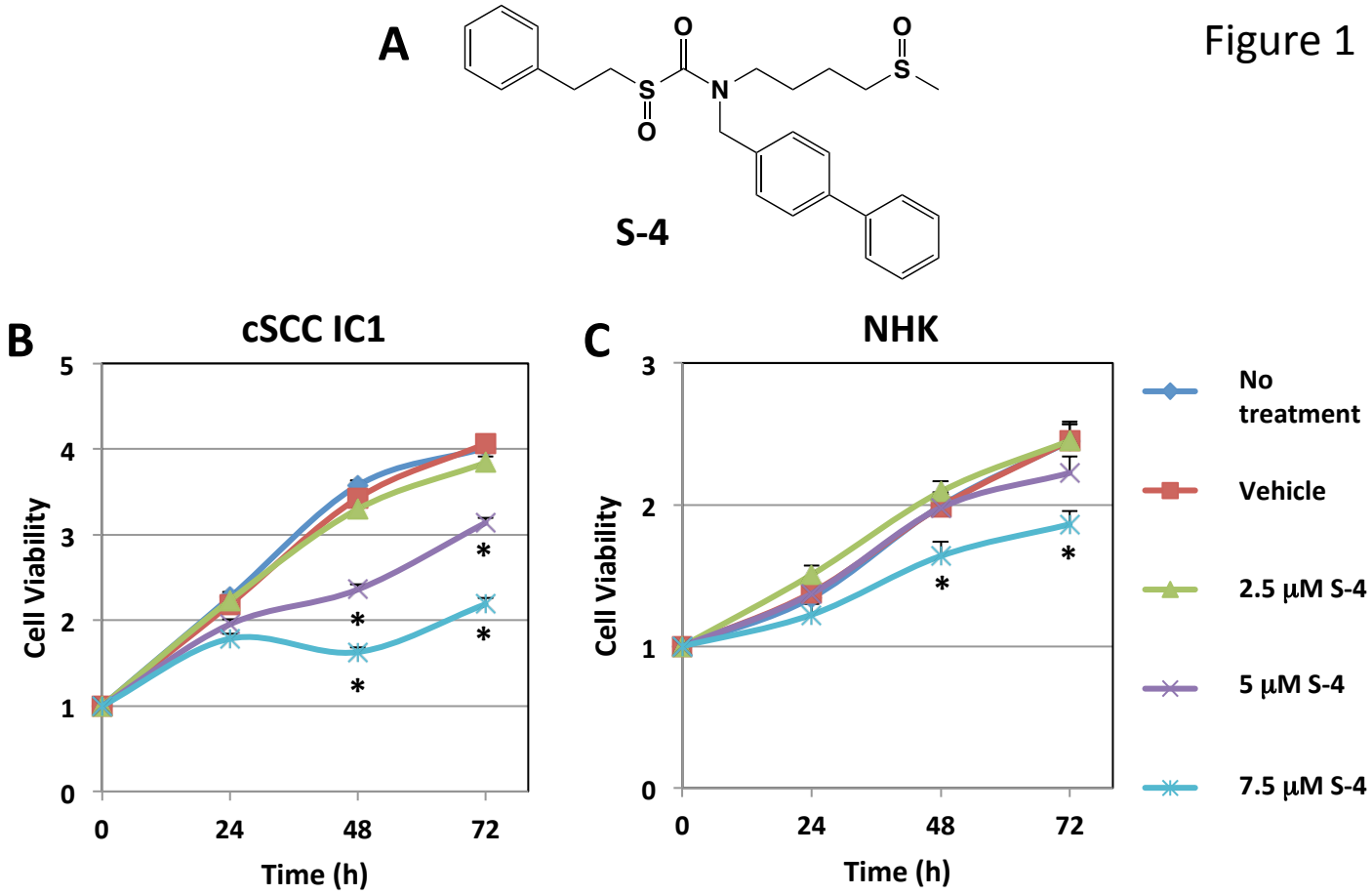
A
S-4
B
cSCC IC1
Cell Viability
Time (h)
C
NHK
Cell Viability
Time (h)
No treatment
Vehicle
2.5 μM S-4
5 μM S-4
7.5 μM S-4
D
S-4 (μM) 0 1.25 2.5 5.0 7.5 10.0
HSP70
GADPH
24h
E
Vehicle
S-4
HSP70
β-Actin
pHSF1 (S326)
β-Actin
Time (h)
0 2 4 8 24

Figure 2

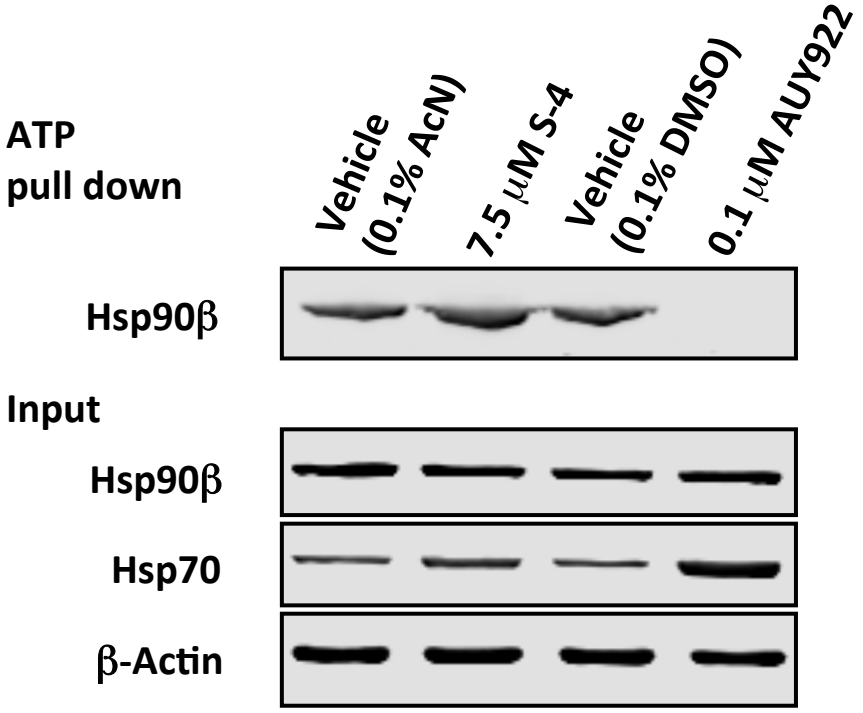
ATP
pull down
Vehicle
(0.1% AcN)
7.5 μM S-4
Vehicle
(0.1% DMSO)
0.1 μM AUY922
Hsp90β
Input
Hsp90β
Hsp70
β-Actin

Figure 3

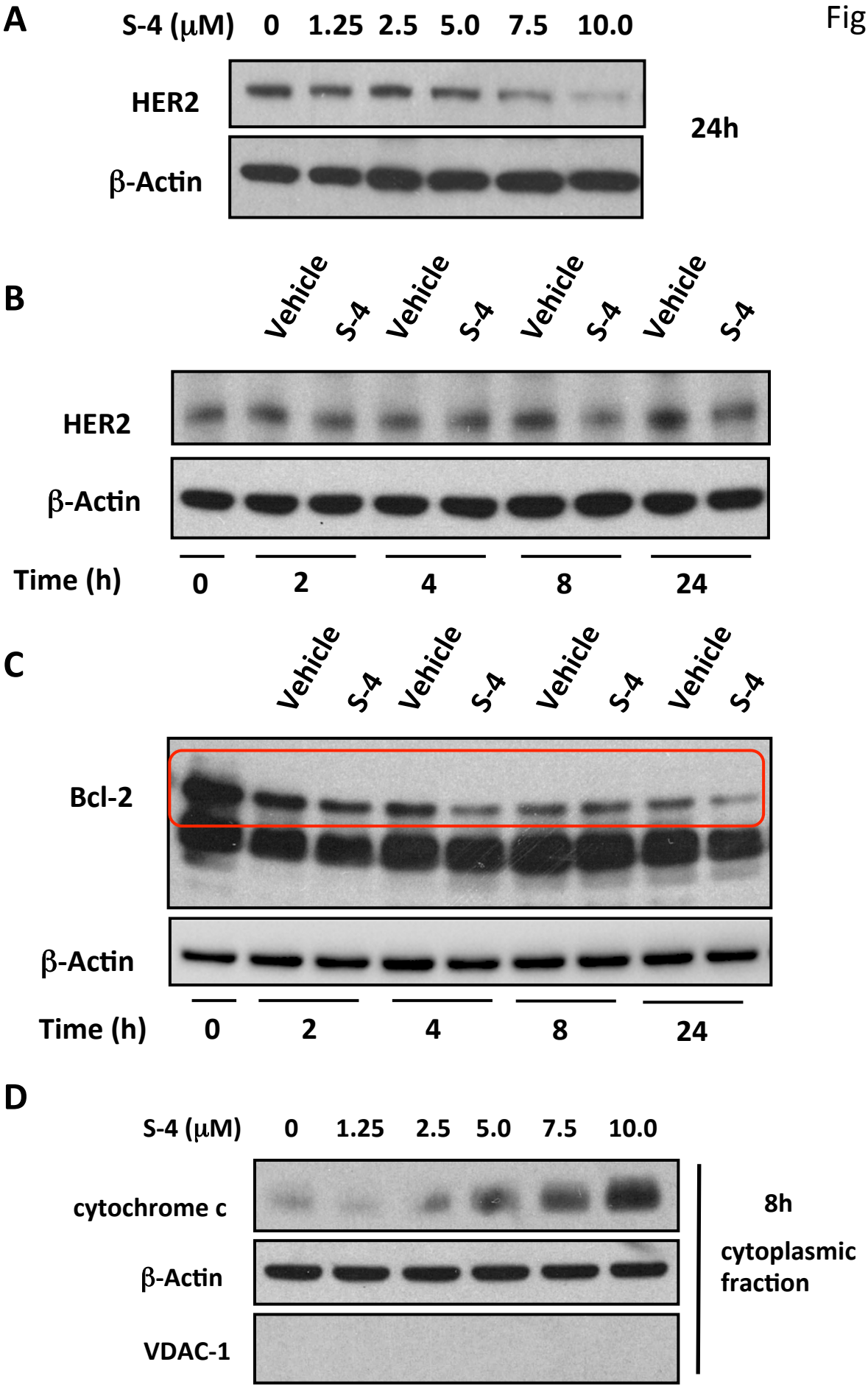
A
S-4 (μM) 0 1.25 2.5 5.0 7.5 10.0
HER2
β-Actin
24h
B
Vehicle
S-4
HER2
β-Actin
Time (h) 0 2 4 8 24
C
Bcl-2
β-Actin
Time (h) 0 2 4 8 24
D
S-4 (μM) 0 1.25 2.5 5.0 7.5 10.0
cytochrome c
β-Actin
VDAC-1
8h
cytoplasmic fraction

Figure 4

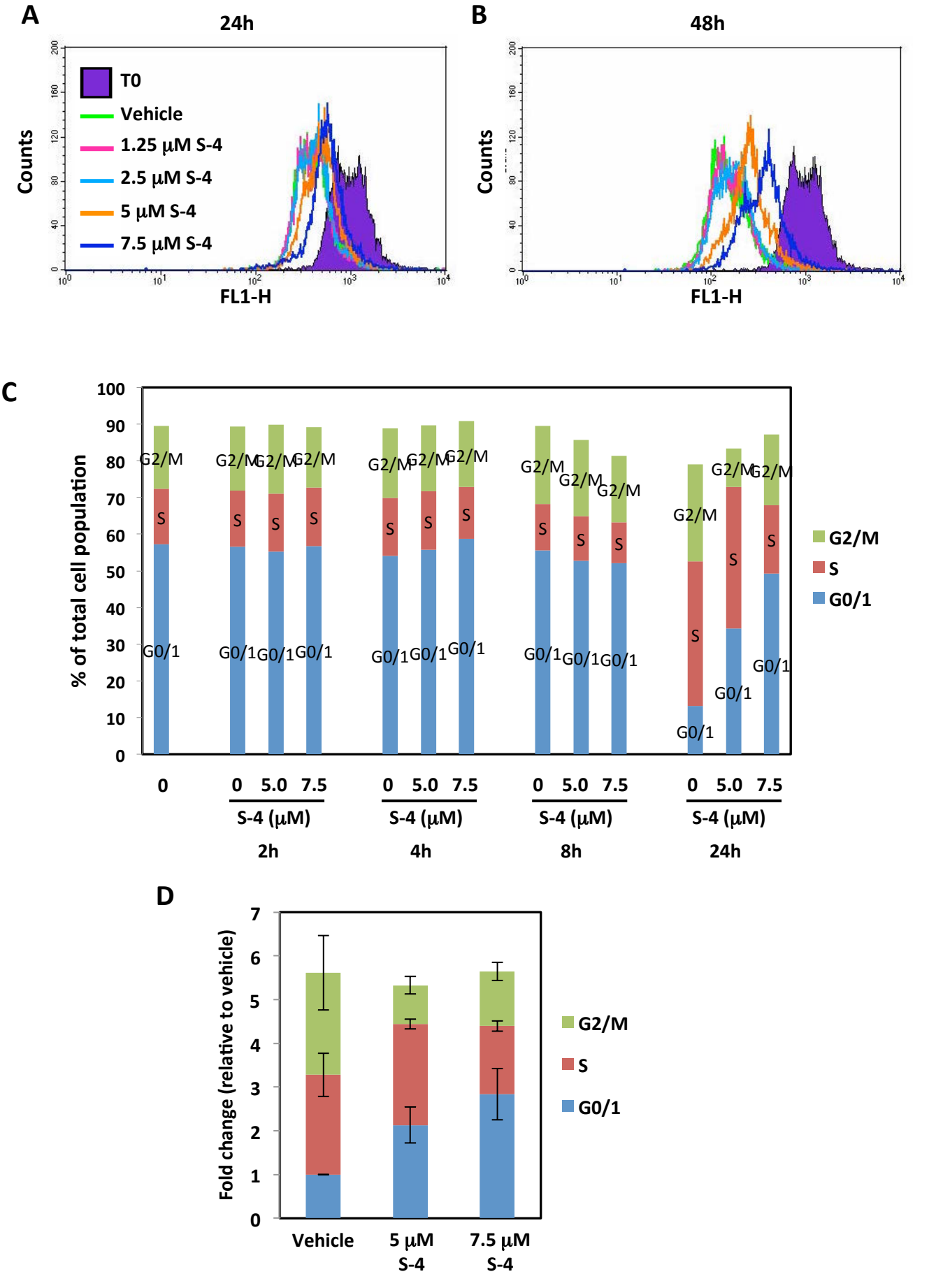
A
24h
T0
Vehicle
1.25 μM S-4
2.5 μM S-4
5 μM S-4
7.5 μM S-4
Counts
FL1-H
B
48h
Counts
FL1-H
C
% of total cell population
G2/M
S
G0/1
0
0 5.0 7.5
S-4 (μM)
2h
4h
8h
24h
D
Fold change (relative to vehicle)
Vehicle
5 μM S-4
7.5 μM S-4
G2/M
S
G0/1

Figure 5

A

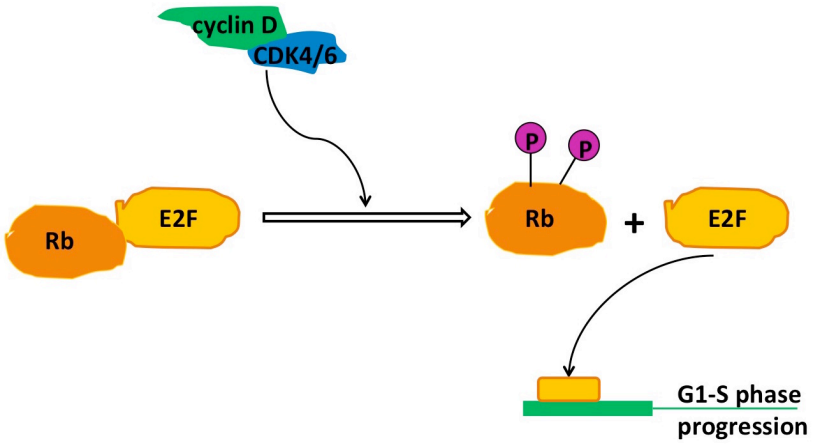
cyclin D
CDK4/6
Rb
E2F
P
P
Rb
+
E2F
G1-S phase
progression

B

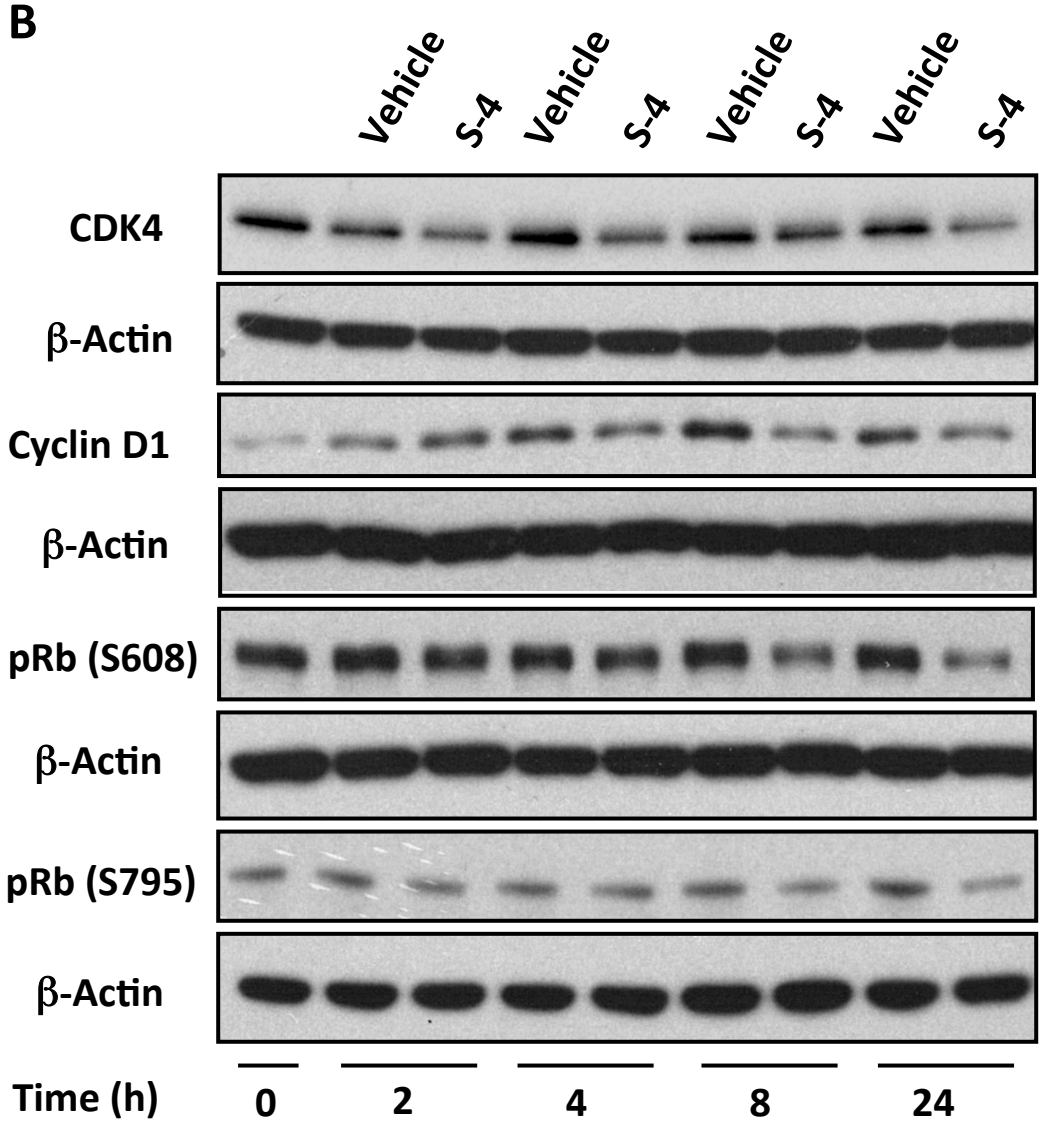
Vehicle
S-4
Vehicle
S-4
Vehicle
S-4
Vehicle
S-4
CDK4
β-Actin
Cyclin D1
β-Actin
pRb (S608)
β-Actin
pRb (S795)
β-Actin
Time (h)
0
2
4
8
24

Figure 6

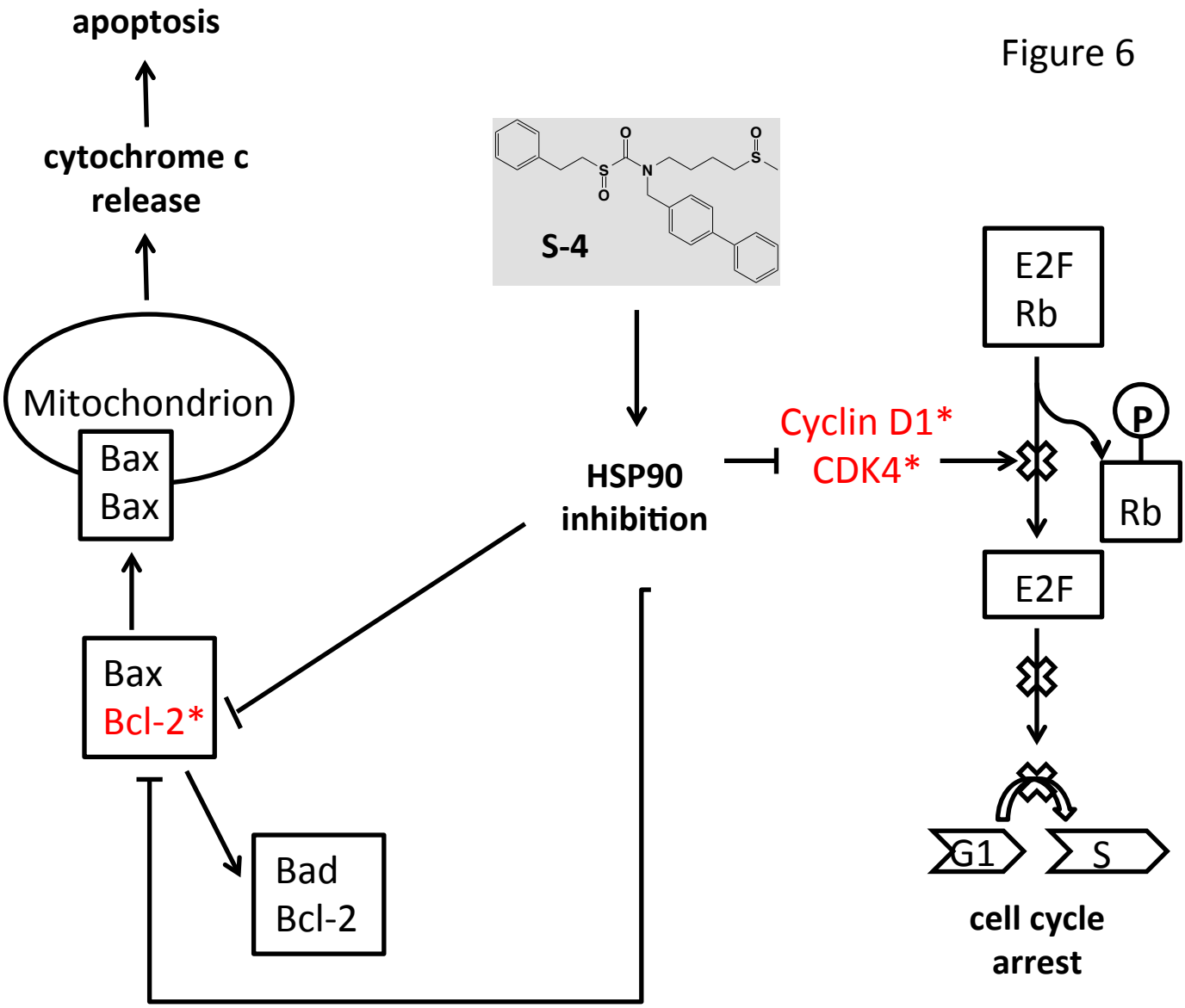
apoptosis
cytochrome c release
Mitochondrion
Bax
Bax
Bax
Bcl-2*
Bad
Bcl-2
S-4
HSP90 inhibition
Cyclin D1*
CDK4*
E2F
Rb
P
Rb
E2F
G1
S
cell cycle arrest

Supplemental Information

Sulfoxythiocarbamate S-4 inhibits HSP90 in human cutaneous squamous cell carcinoma cells

Ying Zhang[1], Young-Hoon Ahn[2], Garrett C. VanHecke[2], Charlotte M. Proby[1], and Albena T. Dinkova-Kostova[1,3]

[1]*Jacqui Wood Cancer Centre, School of Medicine, University of Dundee, Scotland, UK*

[2]*Department of Chemistry, Wayne State University, Detroit, MI, USA*

[3]*Department Pharmacology and Molecular Sciences and Department of Medicine, Johns Hopkins University School of Medicine, Baltimore, MD, USA*

Supplemental Table

Table S1. Modified peptides identified by liquid chromatography-mass spectrometry (LC-MS) after incubation of recombinant HSP90β with S-4 followed by trypsin digestion.

Experimental mass (Da)	Calculated mass (Da)	Peptide score	Peptide sequence	Modifications
2702.1883	2701.2049	45.33	LVSSPCCIVTSTYGWTANMER	Carbamidomethyl (C); S-4 (C)
2717.2013	2717.1998	35.75	LVSSPCCIVTSTYGWTANMER	Carbamidomethyl (C); S-4 (C); Oxidation (M)
2717.2176	2717.1998	27.18	LVSSPCCIVTSTYGWTANMER	Carbamidomethyl (C); S-4 (C); Oxidation (M)
2717.2522	2717.2467	27.61	GFEVVYMTEPIDEYCVQQLK	S-4 (C)
2733.2429	2733.2416	27.78	GFEVVYMTEPIDEYCVQQLK	Oxidation (M); S-4 (C)

Supplemental Figures

Fig S1. Identity and purity of S-4.

(A) ^{1}H-NMR spectrum showing S-4 and traces of residual volatile solvents, ethyl acetate and dichloromethane

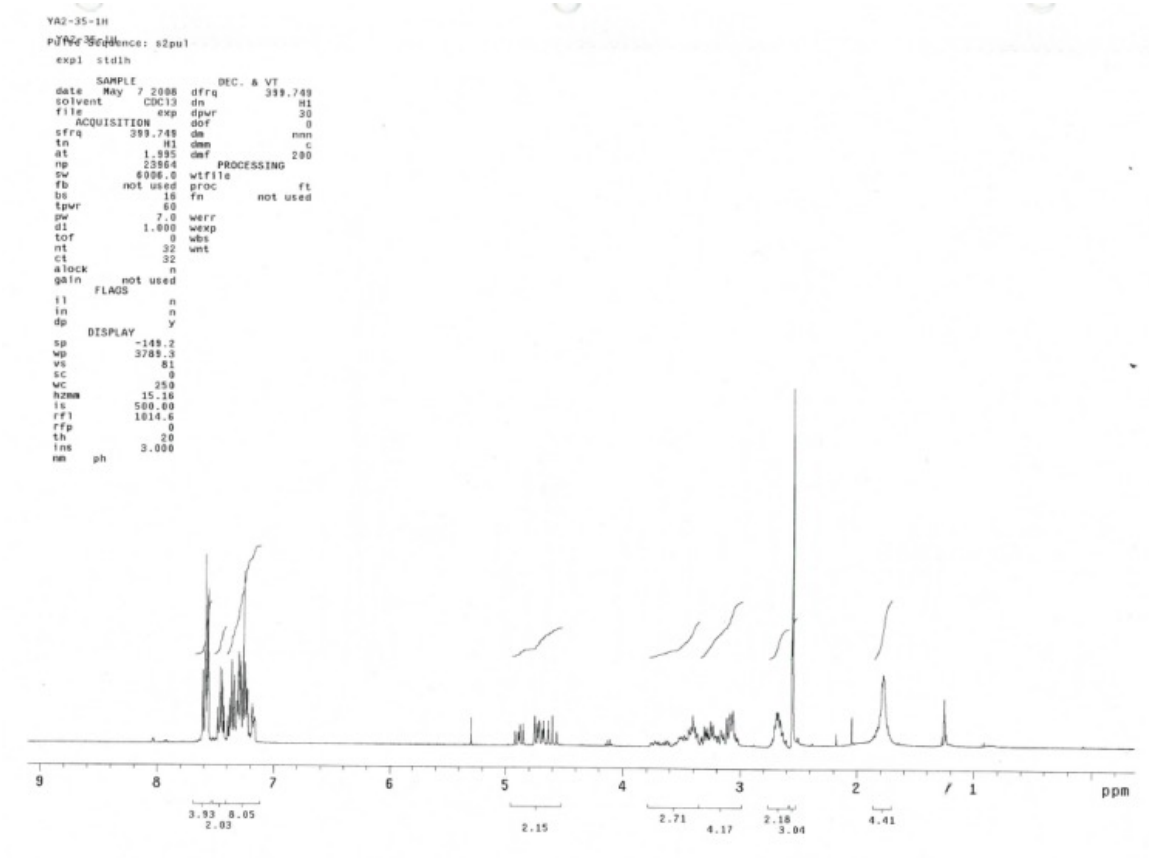

^{1}H-NMR ($CDCl_3$) δ 7.58 (*t*, *J* = 8.4, 4H), 7.45 (*q*, *J* = 6.6, 2H), 7.39-7.16(*m*, 8H), 4.92-4.56 (*m*, 2H), 3.76-3.02 (*m*, 6H), 2.70-2.63 (*m*, br, 2H), 2.55 (*d*, *J* = 1.6, 3H), 1.85-1.74 (br, 4H); ^{13}C-NMR ($CDCl_3$) δ 169.30, 168.86, 141.71, 141.50, 140.54, 140.38, 138.56, 138.49, 134.59, 134.09, 129.15, 129.12, 129.10, 129.09, 129.05, 128.97, 128.92, 128.07, 128.03, 128.01, 127.93, 127.84, 127.30, 127.19, 127.1553.89, 53.79, 53.31, 53.28, 53.14, 51.32, 51.30, 49.53, 49.50, 48.07, 48.03, 45.19, 45.13, 38.88, 38.84, 28.92, 28.23, 28.13, 26.27, 26.21, 20.11, 20.07, 19.98, 19.87.

(B) ^{13}C-NMR spectrum of S-4

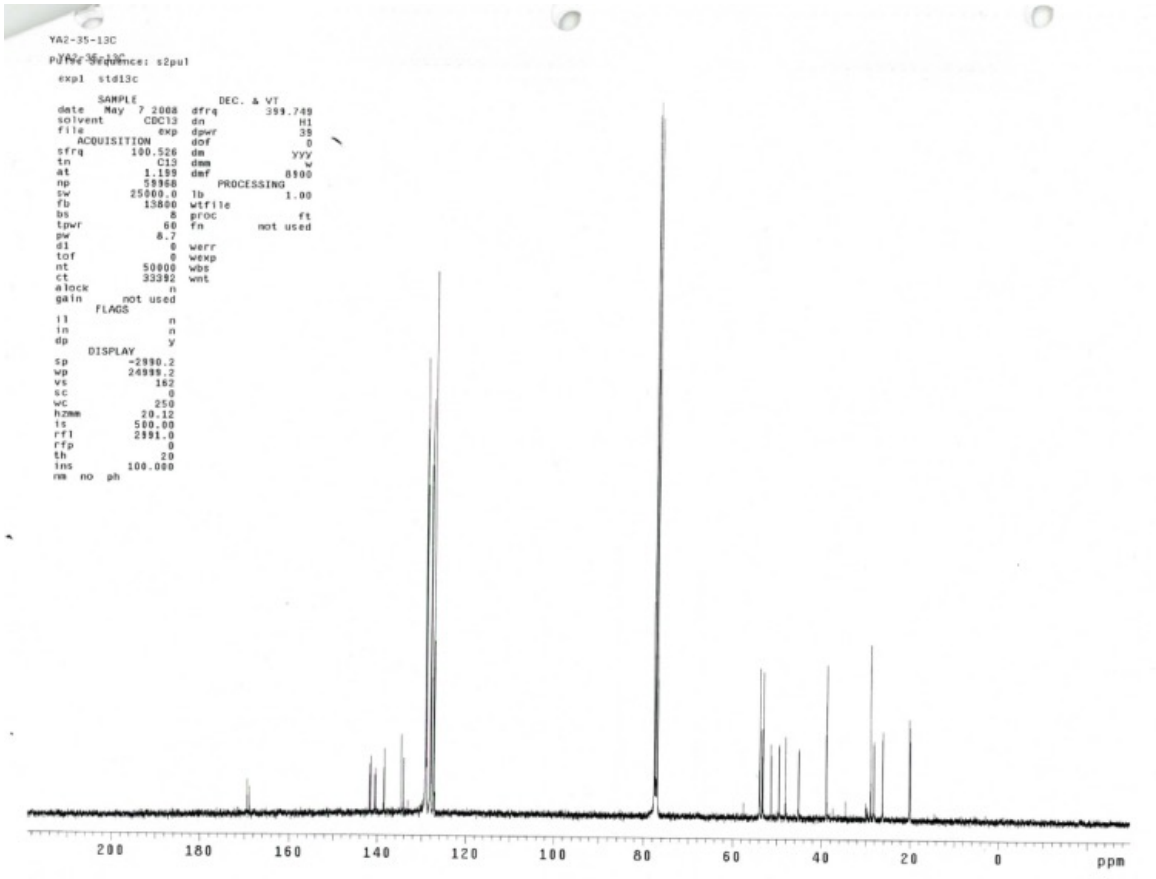

(C) LC analysis of S-4 with UV detection at 254 nm

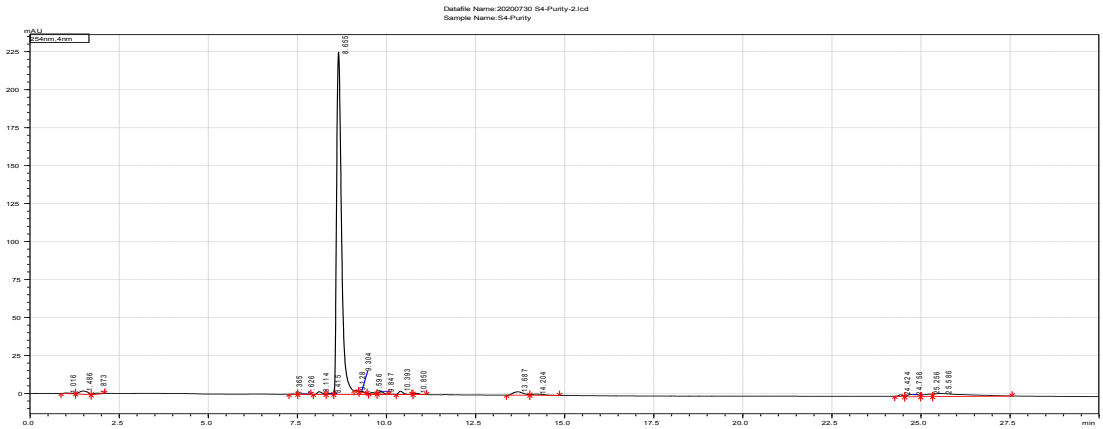

Retention Time	Area	Height	Area%
7.365	1227	193	0%
7.625	2148	243	0%
8.114	15459	1707	1%
8.415	4862	579	0%
8.655	2200107	225668	94%
9.119	1813	354	0%
9.304	4919	763	0%
9.596	7510	817	0%
9.847	13320	1552	1%
10.393	17863	2039	1%
10.85	6480	805	0%
13.688	45637	2241	2%
14.205	19360	786	1%

(D) Positive ESI at 8.6 min (S-4, M = 481.2)

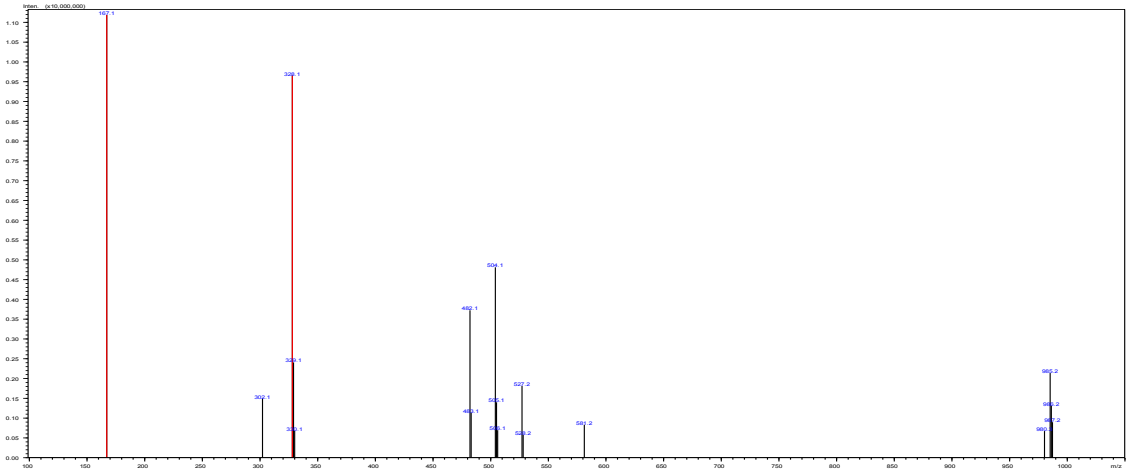

Fig S2. S-4 induces HSP70 and destabilizes the HSP90 client protein HER2 in SCC IC12 cells. Immunoblotting analysis for HSP70 (**A**) and HER2 (**B**) in cells that had been exposed to increasing concentrations of S-4 for 24 h. β-Actin served as the loading control, and acetonitrile (0.1%) served as the vehicle control. Immunoblots are representative of 2 independent experiments.

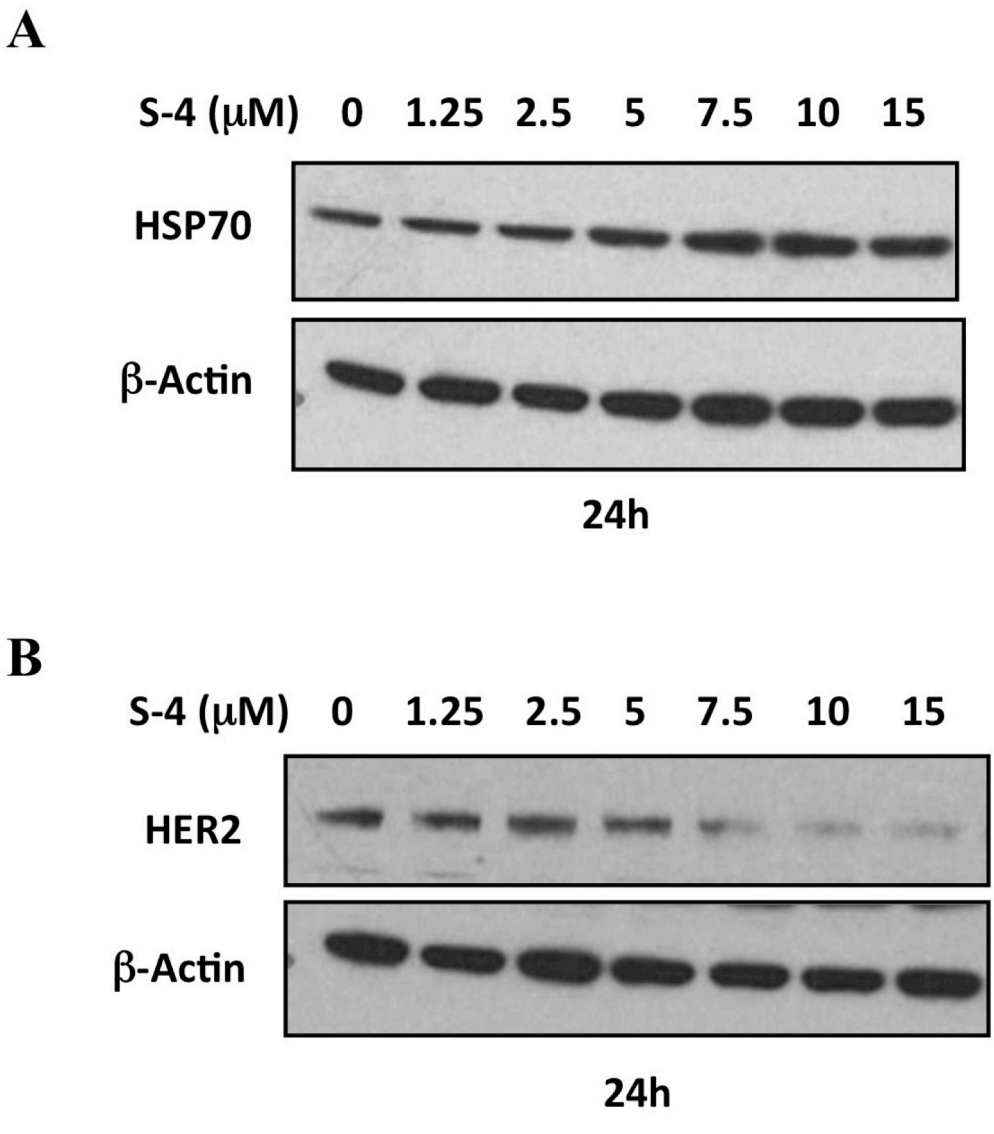

Fig S3. S-4 decreases cell viability and causes cell cycle arrest in SCC IC12 cells.

(**A**) Flow cytometry analysis of SCC IC12 cells that had been labeled with CFSE and treated with vehicle (0.1% acetonitrile) or increasing concentrations of S-4 for 48 h. (**B**) Cell cycle analysis of cells that had been left untreated, or treated with vehicle (0.1% acetonitrile) or S-4 (1.25-, 2.5-, 5-, 7.5-, 10- or 15 μM) for 24 h. Results are representative of 2 independent experiments.